Conference Paper, Published Version

Wang, Weizhi; Pakozdi, Csaba; Kamath, Arun; Bihs, Hans

Large-Scale Wave Modeling for Hydrodynamic Load Calculations on Bridges Foundations in Norwegian Fjords

Coastal Structures 2019 - Nils Goseberg, Torsten Schlurmann (eds) - © 2019 Bundesanstalt für Wasserbau
ISBN 978-3-939230-64-9 (Online) - DOI: 10.18451/978-3-939230-64-9_029

Large-Scale Wave Modeling for Hydrodynamic Load Calculations on Bridges Foundations in Norwegian Fjords

W. Wang, C. Pakozdi, A. Kamath & H. Bihs
NTNU, Trondheim, Norway

Abstract: The E39 coastal highway project aims to build a ferry-free road connection along the west coast of Norway. Several concepts of bottom-based and floating bridges are proposed to connect the deep and wide fjords which have complex bathymetry. Significant water depth variation, deep water condition and irregular coastlines all contribute to the complexity, and challenge the numerical modelling of coastal wave propagation in Norway. Phase-averaged spectral wave models are widely used but face problems representing some wave transformation phenomena such as strong diffraction. Therefore, phase-resolved models are needed for coastal wave modelling. Computational fluid dynamics (CFD) wave models provide highly resolved, accurate phase-resolving simulations for a wide variety of wave hydrodynamic phenomena. However, large-scale coastal wave propagation is typically too computationally demanding using CFD. Numerical models based on shallow water wave theories are more computationally efficient, but the validity of such models is restricted by the deep water condition in the Norwegian fjords. Potential flow models are computationally effective for large-scale long duration coastal wave simulations given that the irregular boundaries are well represented. In this paper, the authors present an efficient phase-resolving fully nonlinear potential flow model with efficient and flexible boundary treatments and use the proposed model to study the wave loads variation on the bridge foundations in a coastal area with a complex bathymetry and an irregular coastline. The model is developed as part of the high-performance open-source hydrodynamics program REEF3D. The high-order discretization schemes and parallel computation in REEF3D are also available to the new potential flow model. The complex bathymetry is efficiently represented using the bottom-following sigma-coordinate system. The coastlines are detected based on the bed elevation and water depth. A large-scale 3D simulation over the natural topography of Sulafjord in Norway is presented. The foundations of the bridges are simplified as solid cylinders and the diffraction theory is used for the wave loads calculation. The wave loads variations along the width of the fjord is demonstrated.

Keywords: Coastal Modelling, Potential Flow, Wave Loads, REEF3D

1 Introduction

Coastal wave processes are typically large-scale phenomena. In Norway, with the deep and wide fjords, the coastal wave behavior is especially a function of large space and time scales. As a part of the National Transport Plan (NTP) for 2014-2023, the E39 coastal highway project in Norway aims to build a continuous road connection along the west coast of Norway (Ellevset, 2012), which is to be achieved by constructing bridges at seven major fjords spanning several kilometers with water depths of several hundred meters. For example, the current research object Sulafjord is 3200 m to 5000 m wide and up to 457 m deep. At some locations, the water depth 200 m away from shoreline reach 200 m as well, making a slope of 45 degrees (Wang, et al., 2017). To ensure the structural integrity of the long-span bridges, several proposals of floating bridges are brought up. The floating bridges are more

exposed to hydrodynamic loads. Large-scale wave modelling is crucial for a better understanding of the wave conditions at the bridge site and the wave loads exerted on the bridges.

Wave models that solve the Reynolds-Averaged Navier-Stokes (RANS) equations have been widely used to study wave-structure interaction especially for extreme wave conditions such as breaking waves loads on cylinders (Alagan Chella, et al., 2019). However, for large-scale and long duration simulations at the bridge sites, Navier-Stokes solvers tend to be too computationally demanding.

For large-scale phenomena in the coastal region, the third generation spectral wave models, such as MIKE 21 SW (Warren & Bach, 1992) and Simulating Waves Near shore (SWAN) (Booij, et al., 1999) are widely used. Both MIKE 21 SW and SWAN give good results for wave energy distribution. However, as phase-averaged wave models, some non-linear phenomena such as strong diffraction cannot be well represented (Thomas & Dwarakish, 2015). Therefore, phase-resolved models are required for wave modelling in areas where strong diffraction takes place due to the irregular shoreline. Shallow water models, such as Boussinesq-type models (Madsen, 1991) (Nwogu, 1993) are fast alternatives for most coastal areas. However, due to the existence of the fjords in Norway, the coastal waters are very deep with sharp gradients in the bathymetry, making it inappropriate to apply shallow water models. Several three-dimensional potential flow models are developed for large-scale long-duration simulations for a wide range of water depths. HOS (Bonnefoy, et al., 2009), OceanWave3D (Engsig-Karup, et al., 2009) and HAWASSI (van Groesen & Andonowati, 2011) are among the most used models of the kind. However, the inclusion of the irregular boundary has remained a challenge, especially for the large water depth change and irregular coastlines in the Norwegian fjords. One recent development in potential flow model is REEF3D::FNPF (Bihs, et al., 2019) based on the open-source hydrodynamic framework of REEF3D (Bihs, et al., 2016). REEF3D uses high-order discretization schemes in space and time and supports parallel computation. The model has been used for many applications, for example, wave interaction with surface piercing cylinders (Kamath, et al., 2015), extreme wave generation (Bihs, et al., 2019), free falling objects into water (Kamath, et al., 2017), local scour around a pipeline (Ahmad, et al., 2019) and new developments of a non-hydrostatic Navier-Stokes solver (Bihs, et al., 2019). As part of the REEF3D framework, REEF3D::FNPF inherits all the high-order schemes and parallel computation capacity. The model solves the Laplace equations for the flow potential together with the nonlinear kinematic and dynamic free surface boundary conditions. The model has been used for simulations of waves propagating over irregular bottom and irregular coastlines (Bihs, et al., 2019) (Wang, et al., 2019) and hence it is chosen for the studies in this paper.

For slender cylinders, with the cylinder diameter to wavelength ratio smaller than 0.2 (D/L<=0.2) (Faltinsen, 1990), the Morison equations (Morison, 1950) are valid and widely used. However, when the diameter to wavelength ratio becomes larger, the diffraction of waves becomes dominant, in which case the diffraction theory needs to be applied for force calculation. A linear diffraction theory (MacCamy, 1954) was developed to be applied for waves with relatively small steepness. For an irregular wave field, some high frequency components have relatively short wavelength in comparison to the dimension of the structure, a diffraction theory is considered more realistic in this regard.

In this paper, the fully nonlinear potential flow model REEF3D::FNPF is used to simulate coastal waves on a large spatial scale and calculate the forces exerted on the hypothetical foundations of a long-span bridge. An array of bridge foundations is modelled as fixed large-radius surface-piercing cylinders in the water. These cylinders are located at one of the proposed fjord-crossing locations together with the natural topography of the fjord. The large-scale numerical simulation of the wave propagation in the fjord provides the hydrodynamic parameters and the wave loads are calculated using the linear diffraction theory. The variation of the wave forces on the cylinders at different locations along the chosen cross-section of the fjord is investigated.

2 Numerical Model

2.1 Governing equations

The numerical wave model solves the Laplace equation and the nonlinear kinematic and dynamic free surface boundary conditions for the flow potential and the pressure field. The governing Laplace equation is as the follows:

$$\frac{\partial^2 \phi}{\partial x^2} + \frac{\partial^2 \phi}{\partial y^2} + \frac{\partial^2 \phi}{\partial z^2} = 0 \quad (1)$$

Boundary conditions are required in order to solve for the velocity potential ϕ from this elliptic governing equation, especially at the free surface and at the bed. The fluid particles at the free surface should remain at the surface where the pressure in the fluid should be equal to the atmospheric pressure. These conditions must be fulfilled at all times and they form the kinematic and dynamic boundary conditions at the free surface respectively:

$$\frac{\partial \eta}{\partial t} = -\frac{\partial \eta}{\partial x}\frac{\partial \tilde{\Phi}}{\partial x} - \frac{\partial \eta}{\partial y}\frac{\partial \tilde{\Phi}}{\partial y} + \tilde{w}\left(1 + \left(\frac{\partial \eta}{\partial x}\right)^2 + \left(\frac{\partial \eta}{\partial y}\right)^2\right), \quad (2)$$

$$\frac{\partial \tilde{\Phi}}{\partial t} = -\frac{1}{2}\left(\left(\frac{\partial \tilde{\Phi}}{\partial x}\right)^2 + \left(\frac{\partial \tilde{\Phi}}{\partial y}\right)^2 - \tilde{w}^2\left(1 + \left(\frac{\partial \eta}{\partial x}\right)^2 + \left(\frac{\partial \eta}{\partial y}\right)^2\right)\right) - g\eta. \quad (3)$$

where $\tilde{\Phi} = \Phi(\mathrm{x}, \mathrm{y}, \eta, \mathrm{t})$ is the velocity potential and $\tilde{w}$ is the vertical velocity at the free surface $\eta(x, y, t)$. At the bottom, the vertical water velocity must be zero at all times and this gives the bottom boundary condition:

$$\frac{\partial \Phi}{\partial z} + \frac{\partial h}{\partial x}\frac{\partial \Phi}{\partial x} + \frac{\partial h}{\partial y}\frac{\partial \Phi}{\partial y} = 0, \; z = -h \quad (4)$$

where $h = h(x, y)$ is the water depth measured from the still water level to the seafloor. The Laplace equation, together with the boundary conditions are solved with a finite difference method on a sigma-coordinate. The transformation from a Cartesian grid to a sigma-coordinate is expressed as follows:

$$\sigma = \frac{z + h(x,y)}{\eta(x,y,t) + h(x,y)} \quad (5)$$

Once the velocity potential Φ is obtained in the sigma-domain, the velocities can be calculated as follows:

$$u(x, y, z) = \frac{\partial \Phi(x,y,z)}{\partial x} = \frac{\partial \Phi(x,y,z,\sigma)}{\partial x} + \frac{\partial \sigma}{\partial x}\frac{\partial \Phi(x,y,\sigma)}{\partial \sigma}, \quad (6)$$

$$v(x, y, z) = \frac{\partial \Phi(x,y,z)}{\partial y} = \frac{\partial \Phi(x,y,z,\sigma)}{\partial y} + \frac{\partial \sigma}{\partial y}\frac{\partial \Phi(x,y,\sigma)}{\partial \sigma}, \quad (7)$$

$$w(x, y, z) = \frac{\partial \Phi(x,y,z)}{\partial z} = \frac{\partial \sigma}{\partial z}\frac{\partial \Phi(x,y,\sigma)}{\partial \sigma}. \quad (8)$$

The sigma-coordinate follows the water depth changes, making the model very flexible regarding bathymetry changes. The coastline is detected based on the bed elevation and the water depth. A relaxation zone is arranged along the coastline so that the reflective property of the beaches can be accounted for based on local scenarios.

The 3rd order TVD Runge-Kutta (Shu & and Osher, 1988) time discretization is used with constant CFL number of 1.0. The derivatives of the velocity potential in the governing equation are estimated using the second-order central differential scheme and the spatial derivatives in the free surface boundary conditions are calculated by the use of the WENO scheme (Jiang & and Shu, 1996)

The model is fully parallelized following the domain decomposition strategy where ghost cells are used to exchange information between adjacent domains. These ghost cells are updated with the values from the neighboring processors using MPI (Message Passing Interface).

2.2 Irregular wave generation

The generation and absorption of the waves is achieved with the relaxation method (Mayer, et al., 1998). The relaxation function proposed by (Mayer, et al., 1998) and (Jacobsen, et al., 2012)is used in the model:

$$\Gamma(\tilde{x}) = 1 - \frac{e^{\tilde{x}^{3.5}} - 1}{e - 1} \; for \; \tilde{x} \in [0; 1] \quad (9)$$

The JONSWAP spectrum recommended by DNV-GL is used as the input power spectrum:

$$S(\omega) = (1 - 0.287\ln(\gamma))\frac{5}{16}{H_s}^2{\omega_p}^2\omega^{-5}exp\left(-\frac{5}{4}\left(\frac{\omega}{\omega_p}\right)^{-4}\right)\gamma^{exp\left(-0.5\left(\frac{\omega-\omega_p}{\sigma\omega_p}\right)^2\right)} \quad (10)$$

Where γ is the non-dimensional peak shape parameter, here $\gamma = 3.3$, σ is the spectral width parameter:

$$\sigma = \begin{cases} 0.07, \ if\ \omega \leq \omega_p \\ 0.09, \ if\ \omega \leq \omega_p \end{cases} \quad (11)$$

A directional spreading function (Mitsuyasu, 1975) is used to represent the multi-directional wave field together with the power spectrum.

$$G(\beta) = G_0(s)cos^{2s}(\frac{\beta}{2}) \quad (12)$$

$$G_0(s) = \frac{1}{\pi}2^{(2s-1)}\frac{\Gamma^2(s+1)}{\Gamma(2s+1)} \quad (13)$$

Where β is the direction of each wave component, Γ is the Gamma function, s is the shape parameter.

The wave condition at Sulafjord is typically a mixture of ocean swell and local wind generated waves. Therefore, a narrow spreading sea-state is simulated with the shape parameter $s = 20.0$.

An equal energy method is used to discretize the power spectrum and the directional spreading function to ensure the ergodicity of the wave field. In the presented study, 100 frequency components are used for the power spectrum and 20 directions are used for the spreading function.

2.3 *Force calculation*

Mac-Camy and Fuchs's theory is used to calculate the wave force on the cylinders (Herbich, 1999):

$$F_x = \frac{4\rho gAtanh(kd)}{k^2H_1^{'}(ka)} \quad (14)$$

Where $H(ka)$ is the first-kind Hankel function of order n, $H_n = J_n + iY_n$, with J_n being the first-kind Bessel function and Y_n being the second-kind Bessel function.

2.4 Numerical tank setup

The chosen site of study is Sulafjord on the west coast of Norway. The waves coming into the fjord are typically a mixture of ocean swell and local wind generated short-crested waves. Floating bridge concepts are proposed where the floating bridges or submerged-tube bridges are supported by an array of platoons. However, for simplicity, only gravity-based foundations are studied in this case, where the foundations are modelled as bottom-fixed surface-piercing cylinders. The surrounding area near Sulafjord is shown in Fig.1 (a) and the proposed fjord-crossing locations are illustrated in Fig.1 (b). The red arrow in Fig.1 (a) indicates the most dangerous wave direction for structures in the fjord. The selected computational domain is shown as a black box in Fig.1 (a) so that all the possible fjord-crossing locations are included and the inlet wave boundary aligns with the direction of the most dangerous wave. The fjord-crossing location in the middle of all three options shown in Fig.1 (b) is the focus of this study. Five cylinders with the radius $a = 40\ m$ are located along the cross-section of this fjord-crossing site.

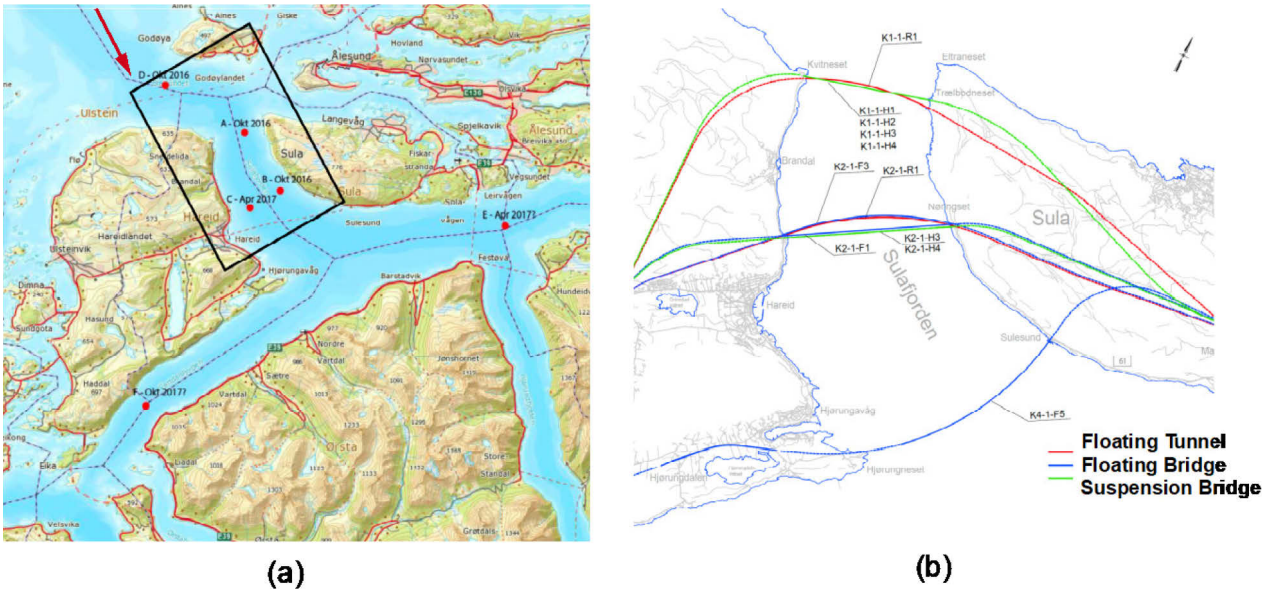

Fig. 1. Overview of Sulafjord in western Norway. (a) the map of Sulafjord. The red arrow indicates the most dangerous wave direction and the black box represents the modelled area in the numerical wave tank.

3 Results

The resulting numerical wave tank is 10000 m long, 9000 m wide with a maximum depth of 457 m. The irregular bathymetry is modelled in the numerical wave tank, as shown in Fig. 2. The input wave has a significant wave height $H_s = 5.2\ m$ and a peak period $T_p = 18.0\ s$. At the inlet boundary, waves are generated with a relaxation zone of 550 m, slightly longer than the wave length calculated with the peak period using deep water linear wave theory. At the outlet of the numerical wave tank, a relaxation zone of 550 m is used to mitigate wave reflection. The coordinates of the wave gauges G0 – G5 are shown in Table 1. G0 is very close to the wave generation zone, G1-G5 correspond to the locations of the cylinders. The angular frequency range of $[0.2, 1.2]\ rad/s$ is chosen so that 99% of wave energy is included. With 35 grids per wavelength, the horizontal grid size $dx = 12.5\ m$ is used. In the vertical direction, 15 sigma-grids are used with a stretching factor of 1.9. With this configuration, the total number of grids in the numerical wave tank is 9.2 million. The simulation time is 3000 s, of which the statistical wave properties are calculated using the data from the last half an hour simulation, i.e. from 1200 s to 3000 s.

Tab. 1. Locations of the wave gauges and the wave properties from the simulation at each location

	x	y	H_s	T_p
G0	600.0	3850.0	5.24	18.00
G1	7650.0	2475.0	1.31	18.37
G2	7650.0	3200.0	2.88	17.48
G3	7650.0	4125.0	3.84	17.48
G4	7650.0	5275.0	4.73	17.83
G5	7650.0	5825.0	1.83	17.65

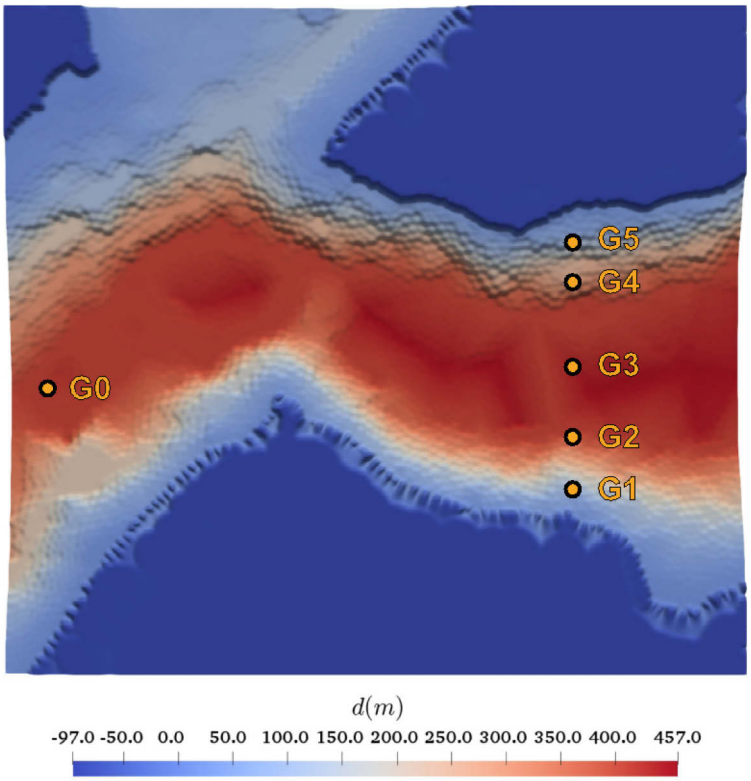

Fig. 2. Bathymetry at Sulafjord modelled in the numerical wave tank and the location of the wave gauges. G1 - G5 represent the locations of the cylinders.

The simulated significant wave heights and peak periods at all wave gauges are listed in Table 1. As can be seen, the wave properties at G0 are nearly identical to the input waves, indicating an accurate wave generation. The simulated wave field with the horizontal velocity in the x-direction is shown in Fig. 3. The irregular waves undergo different wave transformations as they propagate into the fjord. At the entrance of the fjord, the waves shoal near the shoreline and this results in higher waves. The wave direction also changes following refraction due to the varying water depth and diffraction due to the shoreline. The wave field starts to be inhomogeneous when the waves enter the channel of the fjord. As a result, some regions of the fjord have higher waves than other locations, for example wave height at G4 is seen to be higher than G1-G3. This variation is a result of complex wave-boundary interaction and wave-wave interaction and does not show a direct correlation to the local water depth.

The wave forces are calculated at G1-G5 using the linear diffraction theory with the local H_s, T_p and water depth d. It is found that the maximum wave force occurs at cylinder G4. In order to offer a more intuitive comparison, the wave forces and water depth at different locations are normalized by the quantities at G4. The variations of the normalized wave force and local water depth are shown in Fig. 4. Even though G2 and G3 are in deeper water than G4, they are not exposed to higher waves since they are located in a more sheltered area due to the island near the southern boundary. Similarly, G1 and G5 are also at relatively protected area. Consequently, there is no prominent shoaling near G1 and G5 despite that they are located at much shallower water. Comparatively, it is seen from Fig. 2 that the incoming wave group and the diffracted wave group form a field of high waves which leads to the location of G4, causing larger significant wave height there than any other locations along the cross-section. However, the relatively smaller wave height than the input wave is presumably the result of breaking waves near the entrance of the fjord where large and steep waves are observed.

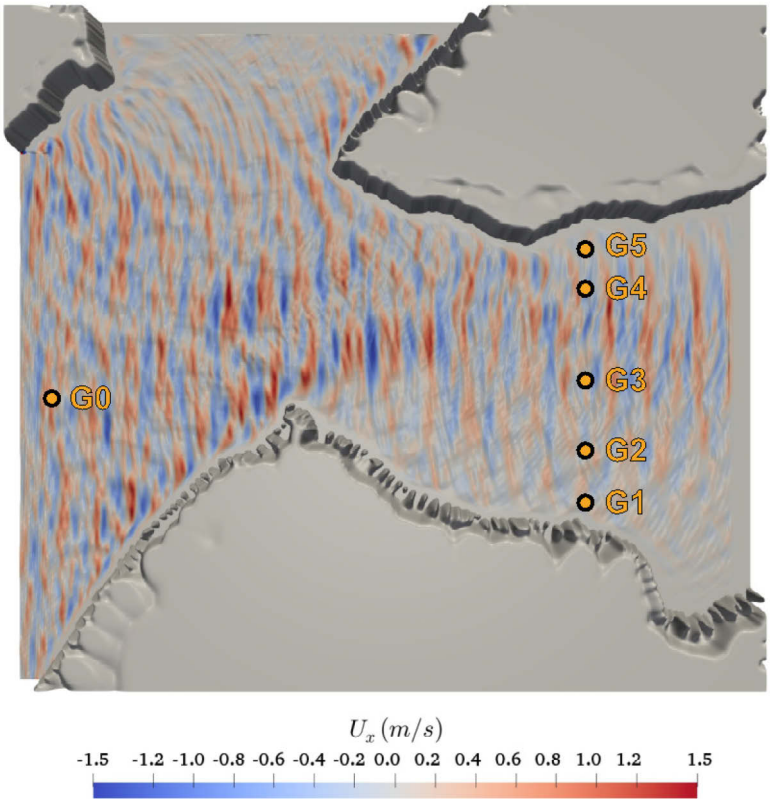

Fig. 3. The simulated narrow spreading wave field at Sulafjord at $t = 3000\ s$. The horizontal velocity component in x-direction is shown.

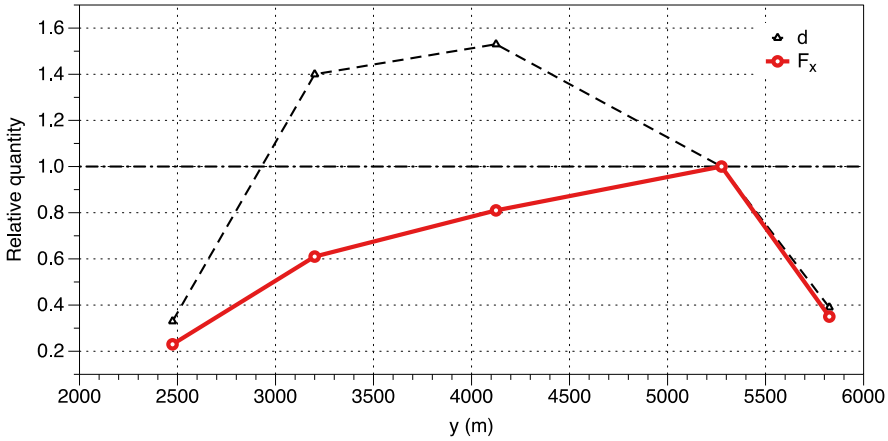

Fig. 4. Variation of the inline force on the cylinders along the chosen cross-section of the fjord. The water depth at the corresponding locations are plotted in the same plot. Both the wave force F_X and water depth d are normalized by the quantities at Gauge 4.

4 Conclusion

A flexible fully nonlinear potential flow solver is used for the simulation of coastal wave propagation in a fjord with an irregular bathymetry with steep gradients and irregular coastlines. A linear diffraction theory is used to calculate the wave loads on hypothetical foundations of a long-span bridge along a cross-section of the fjord. The phase-resolved wave field together with the complicated wave transformation are well represented in the numerical wave tank. The calculated forces at different locations show that the highest wave load is calculated neither where the water is the deepest nor the shallowest region, but in intermediate water depth close to one side of the fjord. The reason is presumably that the diffraction at the entrance of the fjord redistributes the energy of the wave field. As a result, parts of the fjord are sheltered and have smaller waves while other parts have energy

concentration. This distribution of wave energy and wave loads on structures points towards the importance of phase-resolved simulations on a site-specific basis. REEF3D::FNPF has shown the capability of performing such simulations. With different wave conditions, the wave energy and wave load distribution will change accordingly. In the future, different wave steepness, direction spreading functions and locations of the fjord-crossing will be investigated using the proposed numerical model. The force calculation will be improved for the irregular sea state, and more realistic structures will be included for a better representation of real-world scenarios.

5 Acknowledgment

This study has been carried out under the E39 fjord crossing project (No. 304624) and the authors are grateful to the grants provided by the Norwegian Public Roads Administration. This study was supported in part with computational resources at the Norwegian University of Science and Technology (NTNU) provided by The Norwegian Metacenter for Computational Sciences (NOTUR, http://www.notur.no) under project no. NN2620K, http://www.notur.no.

References

Ahmad, N. et al., 2019. Numerical modelling of pipeline scour under the combined action of waves and current with free-surface capturing. *Coastal Engineering,* Volume 148, pp. 19-35.

Alagan Chella, M., Bihs, H. & and Myrhaug, D., 2019. Wave impact pressure and kine- matics due to breaking wave impingement on a monopile. *Journal of Fluids and Structures,* Volume 86, pp. 94-123.

Bihs, H., Kamath, A., Aggarwal, A. & and Pakozdi, C., 2019. Efficient Wave Modeling using Nonhydrostatic Pressure Distribution and Free Surface Tracking on Fixed Grids. *Journal of Offshore Mechanics and Arctic Engineering,* 141(4), p. 041805.

Bihs, H., Kamath, A., Alagan Chella, M. & Arntsen, Ø. A., 2019. Extreme Wave Generation, Breaking, and Impact Simulations Using Wave Packets in REEF3D. *Journal of Offshore Mechanics and Arctic Engineering,* 141(4), p. 041802.

Bihs, H., Kamath, A., Alagan, M. C. & Arnsten, Ø. A., 2016. A New Level Set Numerical Wave Tank with Improved Density Interpolation for Complex Wave Hydrodynamics. *Computers & Fluids,* Volume 140, pp. 191-208.

Bihs, H., Wang, W., Martin, T. & and Kamath, A., 2019. REEF3D::FNPF - A Flexible Fully Nonlinear Potential Flow Solver. *38th International Conference on Ocean, Offshore Arctic Engineering.*

Bonnefoy, F., Ducrozet, F., Le Touze, D. & Ferrant, P., 2009. Time-domain simulation of nonlinear water waves using spectral methods.. *Advances in Coastal and Ocean Engineering,* Volume 11, pp. 129-164.

Booij, N., Ris, R. C. & and Holthuijsen, L. H., 1999. A third-generation wave model for coastal regions, 1. model description and validation. *Journal of Geophysical Research,* Volume 104, pp. 7649-7666.

Ellevset, O., 2012. *Project overview coastal highway route E39,* s.l.: s.n.

Engsig-Karup, A. P., Bingham, H. B. & Lindberg, O., 2009. An efficient flexible-order model for 3D nonlinear water waves. *Journal of Computational Physics,* Volume 228, pp. 2100-2118.

Faltinsen, 1990. *Sea loads on ships and offshore structures.* s.l.:Cambridge University Press.

Herbich, J. B., 1999. *Developments in Offshore Engineering - Wave Phenomena and Offshore Topics.* s.l.:Elsevier.

Jacobsen, N. G., Fuhrman, D. R. & Fredsøe, a. J., 2012. A wave generation toolbox for the open - source CFD library: OpenFoam. *International Journal for Numerical Methods in Fluids,* Volume 70, pp. 1073-1088.

Jiang, G. S. & and Shu, C. W., 1996. Efficient Implementation of Weighted ENO Schemes. *Journal of Computational Physics,* Volume 126, pp. 202-228.

Kamath, A., Bihs, H. & and Arntsen, Ø. A., 2017. Study of Water Impact and Entry of a Free Falling Wedge Using Computational Fluid Dynamics Simulations.. *Journal of Offshore Mechanics and Arctic Engineering,* 139(3), p. 031802.

Kamath, A., Alagan Chella, M., Bihs, H. & Arntsen, Ø. A., 2015. Evaluating wave forces on groups of three and nine cylinders using a 3d numerical wave tank.. *Engineering Applications of Computational Fluid Mechanics,* 9(1), pp. 343-354.

Kamath, A., Alagan, M. C., Bihs, H. & Arntsen, Ø. A., 2017. Energy transfer due to shoaling and decomposition of breaking and non-breaking waves over a submerged bar. *Engineering Applications of Computational Fluid Mechanics,* 11(1), pp. 450-466.

MacCamy, R. C., 1954. *Wave forces on piles: a diffraction theory,* Washington D.C.: Dept. of the Army, Corps of Engineers.

Madsen, 1991. A new form of the Boussi- nesq equations with improved linear dispersion characteristics. *Coastal Engineering,* Volume 15, pp. 371-388.

Mathinsen, T. & Winterstein, S. R., 1992. *On the skewness of random surface waves.* San Francisco, USA, s.n., pp. 472-478.

Mayer, S., Garapon, A. & and Sørensen, L. S., 1998. A fractional step method for unsteady free-surface flow with applications to non-linear wave dynamics. *International Journal for Numerical Methods in Fluids,* Volume 28, pp. 293-315.

Mei, C. C. & Benmoussa, C., 1984. Long waves induced by short wave groups over an uneven bottom. *J. Fluid. Mech., 139,* pp. 219-235.

Mitsuyasu, H., 1975. Observations of the directional spectrum of ocean waves using a clover-leaf buoy. *Journal of Physical Oceangraphy,* pp. 750-760.

Morison, J. R., 1950. The force exerted by surface waves on piles. *Journal of Petroleum Technology,* Volume 2, p. 418–423.

Nwogu, O., 1993. Alternative form of Boussinesq equations for nearshore wave propaga- tion. *Journal of Waterways, Port, Coastal, and Ocean Engineering,* 6(119), pp. 618-638.

Sharma, J. & Dean, R. G., 1981. Second-order directional seas and associated wave forces. *J. Soc. of Petr. Eng., SPE,* pp. 129-140.

Shu, C. W. & and Osher, S., 1988. Efficient Implementation of Essentially Non-Oscillatory Shock Capturing Schemes. *Journal of Computational Physics,* Volume 77, pp. 439-471.

Stansberg, C., 2006. *Laboratory Wave Modelling for Floating Structures in Shallow Water.* Hamburg, Germany, s.n.

Thomas, T. J. & Dwarakish, G., 2015. *Numerical wave modelling a review.* s.l., Aquatic Procedia, pp. 443-448.

van Groesen & Andonowati, 2011. *Time-accurate AB-simulations of irregular coastal waves above bathymetry.* Hong Kong, Proceedings of the Sixth International Conference on Asian and Pacific Coasts (APAC 2011), pp. 1854-1864.

Wang, W., Bihs, H., Kamath, A. & Arntsen, Ø. A., 2017. *Possibilities of CFD Modelling of Deep Water Waves in Sulafjord for The E39 Project.* Trondheim, Proceedings of the ASME 2017 36th International Conference on Ocean, Offshore and Arctic Engineering.

Wang, W., Pakozdi, C., Kamath, A. & Bihs, H., 2019. High performance phase-resolved wave modelling for irregular coastal topography. *10th National Conference on Computational Mechanics.*

Warren, I. & Bach, H., 1992. MIKE 21: a modelling system for estuaries, coastal waters and seas. *Environmental Software,* Volume 4, pp. 229-240.